SAN099-1643J

The diffusion of simple penetrants in tangent site polymer melts

Dana R. Rottach, Patrick A. Tillman, John D. McCoy*

Department of Materials and Metallurgical Engineering

New Mexico Institute of Mining and Technology

Socorro, New Mexico

Steven J. Plimpton and John G. Curro

Sandia National Laboratories**

Albuquerque, New Mexico

* Author to whom mail should be addressed

**Work performed at Sandia National Laboratories supported by the U.S. Department of Energy under Contract No. DE-AC-94AL85000.

DISCLAIMER

Abstract

The diffusive behavior of penetrants in simple polymer melts was investigated by molecular dynamics simulation. For the case where the polymer melt consisted of pearl-necklace chains, the diffusive behavior of the loose pearl penetrants was seen to be qualitatively different than would be expected in realistic models of polymer melts. In particular, there was little or no "non-Fickian" region; the variation of the diffusion coefficient with the penetrant diameter was what one would expect for diffusion through small molecular liquids; and, finally, the long time tail of the velocity auto correlation displayed a "-3/2" power law form, also as in the small molecular liquid case.

When the chains' backbone motion was further constrained by the introduction of a bond angle potential, the qualitative nature of the penetrant diffusion became more "polymer-like". A non-Fickian region developed; the diffusion coefficient varied more rapidly with penetrant diameter; and the velocity autocorrelation function developed a "-5/2" power law tail as would be expected for the diffusion of particles with a wide distribution of trapping times.

1. Introduction

The backbone topology of polymer chains results in the complex self-diffusion behavior seen in polymer melts. This is well known and is qualitatively understood through a reptation perspective. The polymer medium creates a restrictive "tube" about the chain of interest which forbids all but motion along the tube length. One would expect that the diffusion of small molecular penetrants through a polymer melt would be simpler and easier to understand. In particular, since the penetrants have no chain structure, one would expect their motion to have the same power law behaviors as seen in the self-diffusion of small molecular liquids. This expectation turns out to be overly optimistic.

For simulations of realistic systems, a penetrant in a melt is highly trapped by the polymer, apparently as highly trapped in all directions as the polymer chain is in directions perpendicular to the tube. This is not a question of simply reducing the magnitude of the diffusion coefficient; instead, the qualitative nature of the penetrant's motion becomes strongly coupled to the backbone motion of the polymer. Moreover, given the importance of the polymer medium both to the polymer tube formation and to penetrant diffusion, it is possible that penetrant diffusion can be used as a "probe" for exploring the detailed structure of the tube and, in this manner, refining our understanding of polymer self-diffusion.

The more immediate goal of predicting the diffusion coefficient of simple penetrants through a polymer is of great practical importance in such areas as membrane separation and polymer aging. Unfortunately,

the highly trapped nature of the particles makes even this more modest goal virtually unattainable for realistic systems with straightforward simulation techniques because of the long simulation times needed to achieve Fickian behavior [1zz, 2zz]. Consequently, in order to study the diffusion of simple penetrants, indirect approaches have been adopted. For instance, the activation energy of the diffusion constant can be found at high temperatures [3zz] where diffusion is rapid, and used to extrapolate to room temperature, and, even less directly, the polymer medium can be approximated as stochastic in nature [2zz] so that larger time steps may be taken.

An alternative path to the understanding of the mechanisms of penetrant diffusion, and one which we have adopted here, is through the study of simplified polymer models. While such models neglect many molecular details in the interest of computational speed, it is desirable that they retain the correct, qualitative behavior of the diffusive behavior. In the current study, it is demonstrated that simple chain connectivity is not a sufficient condition for the modeling of penetrant diffusion. In particular, we have studied systems where tangent site chains serve as a medium through which simple penetrant sites diffuse and have shown that high chain flexibility results in non-polymeric behavior.

The diffusion coefficient can be determined in several ways. The traditional Fick's law definition of the diffusion coefficient as the proportionality constant relating flux to concentration gradient has recently become more popular [4zz] with the development of hybrid Monte Carlo /

Molecular Dynamics techniques. More commonly, use is made of the equivalent, random walk expression of the diffusion coefficient as the proportionality constant relating the square of the particle's displacement to the time [1zz]. Unfortunately, this relationship only holds at long times and, for polymeric systems, sufficiently long times are often difficult to reach. On more common simulation timescales, penetrants in polymer melts exhibit a "non-Fickian" region where the square of the displacement varies as the square root of time [1zz].

This is similar to the behavior seen in the diffusion of gases through glassy media that arises from the fractal topology of the network of voids [5zz]. While only particles in the percolated network contribute to the long time increase in particle displacement, there are short time contributions from particles in non-percolated networks. As these trapped particles discover the limits of their displacement, the (average) square of the displacement develops a square root of time dependence.

An alternative formalism, that of generalized-hydrodynamics, focuses on the time evolution of the penetrant's velocity [8zz]. Here we focus on the velocity autocorrelation function, Z(t), which is proportional to the average of the dot product of the particle's velocities:

$$Z(t) = \frac{1}{3}\langle \underline{v}(0) \bullet \underline{v}(t) \rangle, \qquad (1.1)$$

At t=0, Z(t) is one third the average of the square of the velocity, and, as a result, this limiting value is dictated by the temperature. At long times Z(t) decays to zero with the details of its decay being associated with more subtle

aspects of the diffusant's motion. Specifically, the diffusion constant, D, is found as the integral of Z(t),

$$D = \int_0^\infty Z(t)dt \qquad (1.2)$$

and, of more importance, an "equation of motion" for Z(t) exists which introduces the concept of a memory function.

The qualitative behavior of the velocity autocorrelation function can be understood by considering two limiting cases. First, when the motion of the penetrant is dictated by small, impulse forces from the medium (that is, in the case of pure Brownian motion), the rate of change of Z(t) is proportional to Z(t) and, consequently, Z(t) is an exponentially decaying function. Low-density gases display a similar behavior although with a power law rather than exponential decay of Z(t).

The second case to consider is the completely trapped particle. A particle in a hard walled sphere is the simplest instance (see the appendix). If the clock is started when the particle has just recoiled from the spherical shell, the dot product of velocities (if it is assumed that the particle passes through the center of the sphere) is a step function as shown in figure 1A. When the product is averaged over all starting points, a spiked behavior is seen as in figure 1B. Finally, by averaging over the Maxwell-Boltzmann velocity distribution with the penetrant's velocity varying the period, a Z(t) is found which decays rapidly and shows a negative well region. This is plotted in figure 1C along with the Z(t) for Brownian motion. Naturally, the diffusion coefficient for a completely trapped particle must be zero and, as a result, the integral of Z(t) for the trapped particle must vanish.

The velocity autocorrelation function for a high-density liquid has similarities to that of a completely trapped particle. In both cases, the function rapidly decays to a minimum then approaches zero. Unfortunately, the velocity autocorrelation function is better at modeling the trapping of a penetrant than its diffusion. If, as is often the case, one is interested in extracting the diffusion constant from Z(t), its long time tail must be known to great accuracy since this is where the non-trapped nature of the diffusant is most fully manifested.

Not surprisingly, the long time tail of Z(t) has been well studied for a number of systems. For atomic liquids [8zz], Z(t) adopts a power law form for long times with an exponent of -3/2 . On the other hand, for locally trapped particles with a wide distribution of trapping times, Kundu and Phillips [7zz] suggest a power law exponent of -5/2. The diffusion of a penetrant in a polymer melt is not clearly one or the other of these. While the local structure is very like a small molecular liquid (suggesting a -3/2 power law decay), the highly trapped nature of the particles suggest a -5/2 power law. We explore this aspect of the penetrant's motion in detail.

Experimentally, neither the velocity autocorrelation function nor the detailed evolution of the particle's displacement can be easily probed. Consequently, the diffusion coefficient remains the primary tool for making contact between theory (or simulation) and experiment. For the simple bead and spring polymer models we consider here, quantitative agreement with experimental diffusion coefficients is, of course, not expected; however, it is desirable that their qualitative natures be similar. In

particular, we will insist that the variation of the diffusion constant with diffusant size be "polymer-like" and not "liquid-like" where "liquid" refers to a small molecular liquid.

The diffusion of penetrants through non-polymeric liquids is relatively well understood. The diffusion constant varies inversely with the penetrant diameter to roughly the 1.8 power as is shown experimentally by the Wilke-Chang [9zz] equation and, theoretically, by Enskog [10zz] theory. This implies that the frequency of a path opening through the penetrant's solvation shell varies roughly as the particle's cross-sectional area; an inference which makes intuitive sense for a "collision-driven" process where the penetrant pushes its way through its neighbors and the neighbors do not show a collective resistance to the penetrant's hop.

For the polymeric case; however, there is a collective resistance. The local compression of the polymer which is needed to permit the penetrant to pass becomes rapidly more difficult as the penetrant's diameter increases. In keeping with this perspective, the diffusion coefficient is found experimentally to vary as the diameter to roughly the seventh power [11zz]. Indeed, the polymer is generally considered to be so stiff that the polymer-penetrant collisions have little effect on the diffusion rate. Instead, the penetrant is viewed as waiting until the polymer's thermal fluctuations cause a sufficiently large hole to open and then hopping through. That is, penetrant diffusion is believed to be an activated process. Not surprisingly, the activation energy is found [12zz] to vary with the penetrant diameter to a power between 1 and 2.

In the remainder of the paper, we explore, in more detail, the effect of chain connectivity and local chain stiffness upon penetrant diffusion. In section 2, the system model is described. Our results are reported in section 3 and conclusions are drawn in section 4.

2. Model and Simulation Methods

The systems investigated were modifications of the pearl necklace chain model which Kremer and Grest [13zz] employed to study polymer dynamics. Previous studies [14zz] have also used this model to study the static structure and thermodynamics of polymer melts and blends. The polymers are modeled as tangent site chains with the bond lengths equal to the site diameter. The bonds are loose springs which permit large timesteps to be taken; however, they are not so loose that chains can cut through each other. The neighboring bonds are encouraged to adopt an angle of 120° by a harmonic potential which is varied in strength from the freely jointed to the freely rotating limits. Non-bonded interactions are repulsive, Lennard-Jones cores, and site diameters are varied by simply shifting the force field to larger (or smaller) separations. In this manner, the penetrant diameters are varied from 80% to 120% that of the polymer site. The larger the diameter, the smaller the diffusion coefficient, and the rate at which D varies with d permits us to comment on the liquid-like or polymer-like nature of the penetrant diffusion process.

The degree of polymerization was fixed throughout at 50 sites per chain, and the total number of independent chains, at 16. Of course, because of the periodic boundary conditions, the number of chains within a

periodic box varied as the chains laced from one box to the next; however, the number of polymer sites remained fixed at 800 per box. In order to mimic experimental systems, the packing fraction was held fixed at 0.465 and the system volume was varied to compensate for the number (5 to 15) and size of the penetrants in the simulation. Explicitly, this is

$$V_{box} = \frac{\pi}{6}\frac{\left(N_P d_P^3 + N_d d_d^3\right)}{\eta_{box}} \tag{2.1}$$

where V_{box} is the volume of the box; η_{box}, the net packing fraction; N_P, the number of polymer sites; N_d, the number of diffusant sites; d_P, the hard site diameter of a polymer site; and N_d, the hard site diameter of a diffusant site. The hard site diameters were calculated through a Barker-Hendersen mapping [15zz]:

$$d = \int \left[1 - \exp\left(-\beta U(r)\right)\right] d\underline{r} \tag{2.2}$$

where U(r) is the non-bonded interactions discussed below; β is 1/kT; k is the Boltzmann constant; and T is the temperature .

Non-bonded polymer sites interacted with each other through a purely repulsive, truncated Lennard-Jones potential,

$$U_{\alpha\beta}(r) = 4\varepsilon\left[\left(\frac{\sigma}{r-\Delta_{\alpha\beta}}\right)^{12} - \left(\frac{\sigma}{r-\Delta_{\alpha\beta}}\right)^{6} + \frac{1}{4}\right] \qquad \text{for } r < 2^{1/6}\sigma + \Delta_{\alpha\beta} \tag{2.3}$$

$$U_{\alpha\beta}(r) = 0 \qquad \text{for } r \geq 2^{1/6}\sigma + \Delta_{\alpha\beta}$$

where the constants σ and ε define the energy and length scales. In addition, the reduced temperature, kT/ε, is unity, and, since all lengths are expressed in terms of σ, it may also be treated as being unity. The penetrant size is varied through the term $\Delta_{\alpha\beta}$, which, in effect, defines the difference between the polymer and penetrant diameters. Consequently, $\Delta_{\alpha\beta}$ is 0 for polymer-polymer (pp) interactions and varies with the size of the penetrant. The Δ for polymer-penetrant interactions is given by Δ_{pA} which is half the penetrant-penetrant Δ_{AA}.

In addition to the above interactions, bond lengths were constrained through the FENE potential,

$$U_{bond}(r) = -0.5HR_0^2 \ln\left[1-\frac{r}{R_0}\right] \quad \text{for } r < R_0$$
$$U_{bond}(r) = \infty \quad \text{for } r \geq R_0 \qquad (2.4)$$

As in Grest and Kremer's work [13zz], H=30, and R_0=1.5. The combination of the two above potentials produces a loose spring centered at 1.0 for bonded polymer sites. Further backbone constraints are included by a harmonic bond angle constraint:

$$E = K(\theta - \theta_o)^2 \qquad (2.5)$$

where θ is the bond angle and $\theta_o = 2\pi/3$ (i.e., 120°). The stiffness parameter, K, is varied (in units of kT) from 0 to 500, which spans the range from freely jointed to freely rotating backbones. For K=0, a single site can respond to a

local perturbation, but, as the stiffness is increased, more of the chain backbone is affected by the motion of a single site. In other words, the constraints on a polymer site become delocalized along the backbone.

Although the K=0 to 500 variation is intended to be smooth, a mild symmetry breaking results from the introduction of the 120° biasing of the bond angle; a biasing which does not exist for K=0. The properties of systems with small values of K are little different than K=0 systems, and we conclude that the system properties do, indeed, vary smoothly with K as K becomes non-zero.

The small molecule diffusants were modeled as free (unattached) monomers. These interacted with the bonded sites (and each other) through equation (2.3) where the Δ is selected for the appropriate site diameters and ranged from –0.2 to 0.2. If a CH_2 group were of unit diameter, then the van der Waals diameters [16zz] of the permanent gases would span this same range. The dilute diffusant limit is of the most experimental pertinence; however, in the interest of computational efficiency, systems of from 5 to 15 diffusants were studied.

The Molecular Dynamics (MD) methodology [17zz] used in this study was based upon a Verlet algorithm previously implemented for similar studies [14zz]. Even for runs where little or no non-Fickian behavior was evident in the migration of the diffusant particles, relatively lengthy runs were still necessary in order to achieve adequate statistics for the computation of diffusion coefficients. The simulation time-steps were 0.0046 to 0.006 where the time unit is $t_0=\sigma\,(m/\varepsilon)^{1/2}$ and m is the mass of a

site (all sites were of equal mass). A typical long run consisted of $25X10^6$ time steps and $7.5X10^6$ time steps for short runs. The first 30,000 time steps were discarded for equilibration purposes. If the sites were interpreted as CH_2 monomers at, say, 420 K, the length of one of the long simulations would be in the 70 nanosecond range.

Both static and dynamic average quantities were calculated throughout the course of the simulation. First, and most importantly, was the diffusion constant. The positions of the diffusants were periodically noted, and the average displacement of the particles as a function of time computed. Of course, this was an average over initial time as well as over the 5 to 15 penetrants in the system. Typical results are shown in figure 2 for 10 penetrants in K=0 and K=500 polymer melts. In the K=500 case, the small region with a slope approximately one half, spanning between the short time ballistic region (slope = 2) and the long time Fickian region (slope = 1) is the non-Fickian regime. The diffusion constant, D, is found directly from the the Fickian region through the Einstein relationship[9vv],

$$\langle R^2 \rangle = 6Dt \qquad (2.6)$$

where R is the displacement of a penetrant during a time interval t and <..> indicates the average over both initial time and penetrant. In order to apply this for short times which are barely in the Fickian region, it is convenient to evaluate the diffusion constant with the differential form of the above equation,

$$D = \frac{1}{6}\frac{d\langle R^2 \rangle}{dt} \qquad (2.7)$$

which is equivalent to equation (2.6) at long times. In the current study, D is in units of σ^2/t_0 , which is equivalent to $(\varepsilon\sigma^2/m)^{0.5}$, or $(kT\sigma^2/m)^{0.5}$. For the cases in figure 2, the diffusion constants were found to be 0.10±0.01 (for K=0) and 0.011±0.001 (for K=500). If the penetrant were CH_4, the unit of diffusion would be 5 X 10^{-6} cm^2/sec, and the increase in K from 0 to 500 would correspond to a decrease in D from 5X10^{-7} to 5 X 10^{-8} cm^2/sec.

When determining the diffusion coefficients there is a question of what range of times to fit (as it needs to be well past the ballistic and non-Fickian regimes but not so long that there are too few data points to obtain a good average). We chose to fit to the region between 60 and 120 reduced time units. In this region we are looking at displacements in the range of about half the length of the periodic box, or roughly five site diameters.

Interestingly, on a per particle basis, the linearity of the Fickian regime degrades rapidly once a particle has traversed further than a box length. Beyond this point, the particles can be identified as rapid or slow moving. This behavior is indistinguishable from penetrant behavior in glassy polymers where molecules diffusing through percolating networks of voids continue their migration while molecules in non-percolating networks are limited in their ultimate displacements.

This behavior is potentially problematic during the analysis of simulation trajectories. If a diffusive pathway has percolated the length of the periodic box, then, effectively, it is of infinite extent since it can loop back on itself. Consequently, if, as is commonly assumed, a pathway is long lived, any particles in such a pathway would migrate rapidly in a

physically unreasonable manner. On the other hand, this behavior is also in keeping with Wilson, Pohorille and Pratts' [18zz] observation of the effect on diffusive behavior of spurious phonon modes introduced by the finite system size. In either case, it follows that conclusions based upon displacements greater than a box length should be viewed with suspicion.

The idea of a network of latent diffusion paths in a polymer melt is physically appealing. A number of researchers [6zz] have analyzed snapshots of melt simulations and find that there is indeed a clustering of free volume; however, the longevity of these networks has not been systematically explored. On the other hand, Suter et al. [2zz] have used this percolating network model of penetrant diffusion in their stochastic simulation methods to good effect. In addition, the Kundu and Phillips [7zz] treatment of a wide distribution of trapping strengths is also in keeping with the observation of a distribution of trapping environments.

As a practical consequence, the apparent trapping of particles by the polymer matrix causes the evaluation of the diffusion constant to be difficult. Since the diffusion constant is effectively an average over lightly and strongly trapped particles, its value is sensitive to the relative concentration of these particle types. Since only a few penetrants are used in a typical simulation, it is usually not clear that phase space is adequately sampled. Because, in the current study, the displacement trajectories of the penetrants do not diverge until after they are well into the Fickian regime, and because, as shown in figure 2, the subsequent behavior of the

particle average is in keeping with its earlier behavior, we concluded that the MD runs were of adequate length to approach ergodicity.

An alternate way to calculate the diffusion constant is through the velocity autocorrelation function,

$$Z^*(t) = \frac{1}{3}\langle \underline{v}(0) \bullet \underline{v}(t) \rangle / Z(0), \tag{2.8}$$

and the Green-Kubo relation [10zz]

$$\frac{m}{kT} D = \int_0^\infty Z^*(t) dt \tag{2.9}$$

where Z*(t) is the reduced velocity autocorrelation function, and Z(0) is kT/m.

3. Results

In figure 3, the velocity autocorrelation functions for both polymer and penetrant sites are shown for the K=0 system shown in figure 2. As opposed to the simple decay seen in low density systems, these functions show a great deal of structure. Much of the polymer's fine structure results from its bond vibrations. Interestingly, the polymer's vibrational motion is not evident in the penetrant's Z(t) which indicates that while the penetrant may be strongly trapped by the polymer, it is not "bound" to the polymer.

In figure 4, the penetrant's velocity autocorrelation function is integrated for both K=0 and 500 cases where the tail has been fit to a power law form. The diffusion coefficient calculated in this manner is 0.093±0.008

for K=0 and 0.012±0.001 for K=500, both of which are in keeping with their $<R^2>$ based values

For most physical properties, chain connectivity can account for unusual features peculiar to polymeric materials in a qualitative manner. This, however, does not appear to be the case with the diffusion of penetrants. Instead, as seen in figure 5, simple pearl necklace chains provide a diffusive environment similar to that of a low molecular weight liquid. In both cases, the diffusion constant is seen to vary with the penetrant diameter to the -1.8 power.

To understand this similarity, it is necessary to consider the qualitative driving force of diffusion. In low molecular weight liquids, diffusion is "collision driven" where the opening of a diffusion path is tied to the collision rate of the penetrant. In other words, the penetrant helps to punch a hole for itself in the wall of the solvation shell which is attempting to restrict the particle's movement. The resulting diffusive behavior is described empirically by the Wilke-Chang equation [9zz] and theoretically by Enskog (and associated) [10zz] theories. In both cases, approximately a -1.8 power law is predicted.

That penetrant diffusion in pearl necklace chains should exhibit Wilke-Chang behavior is surprising. Apparently, the high, local flexibility of these tangent site chains permits the chains to be highly responsive to the thermal collisions of the penetrants. In particular, a single polymer site can move out of the path of a penetrant, as the result of a collision, without

perturbing the rest of the chain. The fact that the beads are connected does not alter the penetrant diffusion in a qualitative way.

By contrast, in a real polymer, the chain backbone motion is a cooperative process. A single monomer cannot move without also moving other monomers on the backbone. Consequently, the penetrant can be viewed as being completely at the whim of the polymer medium. Cooperative fluctuations of the polymer backbone take place without being substantially affected by the collisions of the penetrant. When a diffusion path, of its own accord, opens beside a penetrant, then a diffusion step may take place.

In real macromolecules, bond angle constraints and rotational potentials ensure that the chain backbone motions are non-local and, consequently, unresponsive to penetrant collisions. This effect can be captured simply through the introduction of the stiff bond angle potential defined in equation (2.5). As the bond angle force constant, K, is increased, the chain is transformed from a freely jointed to a freely rotating backbone. Obviously, the diffusion coefficients of the penetrants are reduced by the more restricted motion of the chains. More importantly, and less obviously, the penetrant's diameter has a stronger effect on D. When a K of 500 is reached, the diffusion coefficient varies with a much steeper apparent power law with an exponent of about -4, and further restrictions on backbone motions would likely increase this exponent. As can be seen in figure 6, this is in much more reasonable agreement with the experimental behavior of polymer melts. In Table 1, the diffusion constants calculated

from equation (2.7) are reported as a function of both penetrant diameter and bond angle stiffness.

Since, based on the above discussion, it seems that a K of 500 is sufficient to result in penetrant diffusion which is "polymer-like", it is of interest to explore the variations in the velocity autocorrelation function as K is varied from 0 to 500. In figure 7, the tail region of Z(t) is shown for K=0 with the full Z(t) in the insert. Clearly, the tail is fit well by a $t^{-3/2}$ form as would be the case for small molecular liquids. On the other hand, the K=500 case shown in figure 8, is very poorly fit by a $t^{-3/2}$ tail while a $t^{-5/2}$ gives excellent agreement with the simulation. The best fit power law exponent is given for each bond force constant and penetrant diameter in Table 2. As a check on our accuracy, we have calculated the diffusion coefficients from the velocity autocorrelation functions using equation (2.9), and these are reported in Table 3. As can be seen in figure 9vv, they are in good agreement with those calculated from the Einstein relation, equation (2.7).

In principle both methods of obtaining the penetrant diffusion constant are equivalent. Use of the Einstein formula, however, obviously requires that the simulation be run long enough to reach the Fickian regime. This was possible for the course grained polymer models studied here, but it is much more difficult to achieve for more realistic models of polymers. Thus the velocity autocorrelation function method provides a feasible alternative for realistic polymer models.

In particular, the velocity autocorrelation route is far more amenable to parallel computation, which can be understood as follows. In order for

$\langle R^2 \rangle$ to yield D, a sufficient number of hops must have occurred for the random walk nature of the diffusive motion to be plain. Since this is roughly 100 hops, there is an inherent $100t_H$ minimum time scale to the method where t_H is the time between hops. Even if the trajectories of many particles are averaged together, simulations of at least 100 t_H must be performed and the system size must be large enough to contain the 100 t_H trajectories. On the other hand, Z(t) has an inherent time scale of the hop time, t_H. Consequently, much shorter simulations are needed to span the time range of interest. Naturally, a single run of length τ would yield poor statistics; however, averages over many short runs, or many penetrants, would dramatically improve the statistics. This suggests an almost trivial parallel computation, where it is often more efficient to do many independent, short runs simultaneously on different processors, rather than one long run of a single system, particularly if the system is of modest size.

It is possible to treat the velocity autocorrelation function using the formally exact, generalized Langevin formulation of particle dynamics [10zz]. Here the rate of change of Z(t), $\dot{Z}(t)$, which is an acceleration of sorts, is related to Z(t) in a manner similar to that of the hydrodynamic deceleration of a classical particle in a liquid with a time dependent friction factor:

$$\dot{Z}(t) = -\int_0^t \varsigma(t-\tau)Z(\tau)d\tau \qquad (3.1)$$

where the "friction factor", $\zeta(t)$, is referred to as the memory function. If Z(t) decays with a power law, as in both the simple liquid-like K=0 case ($t^{-3/2}$) and the freely rotating K=500 case ($t^{-5/2}$), the memory function also decays with the same power law dependence[19zz]. If, instead, the velocity autocorrelation function is that of a Brownian particle, the memory function is a delta function, and equation (3.1) is easily integrated to yield a simple exponential decay in Z(t).

Less intuitively, the memory function can also be expressed as

$$\varsigma(t) = \phi(t) - \frac{1}{Z(0)}\int_0^t \varsigma(t-\tau)\dot{Z}(\tau)d\tau \qquad (3.2)$$

where $\phi(t)$ is the normalized autocorrelation function of the instantaneous force on the particle:

$$\phi(t) = \frac{\langle \underline{F}(t) \bullet \underline{F}(0) \rangle}{m^2 Z(0)}; \qquad (3.3)$$

F(t) is the instantaneous force and m is the particle's mass. Consequently, for short times, the second term in equation (3.2) is small and the memory function approaches the force autocorrelation function. The force autocorrelation function was calculated directly during the MD simulation from the force on the penetrant, and, in figure 10vv, $\phi(t)$ is plotted for both K=0 and K=500. The well depth is seen to increase with K, indicating the development of a more clearly defined solvation shell.

The memory function is often expressed in Laplace space since the transform of equation (3.1) is amenable to a simple algebraic solution:

$$\tilde{\zeta}(p) = \frac{1}{\tilde{Z}(p)} - p \qquad (3.4)$$

where the tilde denotes the Laplace transform of $Z^*(t)$. In figure 11vv, the velocity autocorrelation functions for large K's are seen to develop well defined maxima in p-space. Qualitatively, this behavior may be understood as follows. For a Brownian particle, $\tilde{Z}(p)$ is $1/(p+\zeta_0)$ where $\zeta_0=kT/(mD)$, and, as p approaches zero, $\tilde{Z}(p)$ becomes a constant. Since all diffusant particles behave like Brownian particles at long times (i.e., small p), one would expect $\tilde{Z}(p)$ to approach a constant value as p approaches zero. Of course, as D becomes smaller with increasing K, p must be smaller in order for $\tilde{Z}(p)$ to be approximately a constant. Indeed, for the fully trapped particle of figure 1, the p=0 limit of $\tilde{Z}(p)$ would be zero with no "diffusion dominated" region. On the other hand, for short times (i.e., large p), the penetrant motion is ballistic (with Z(t) ~ constant or $\tilde{Z}(p) \sim 1/p$) and insensitive to the chain stiffness which implies that $\tilde{Z}(p)$ is independent of K at large p. Naturally, the transition between large and small p is complex.

The Laplace transform of the memory function is shown in figure 12vv. The penetrants in a K=0 polymer have memory functions which smoothly switch from small p, diffusive behavior ($\sim p^0$) to large p behavior which indicates that short time trapping effects result in 1/p deviations from ballistic motion. In contrast, the penetrants in a K=500 polymer display a clear intermediate region with a fractional power law behavior.

This intermediate region becomes more prominent in the completely trapped limit, and, as a natural consequence of its growth, the memory function diverges at P=0.

4. Conclusions

In general, we have demonstrated that, even though chain connectivity appears to be a sufficient condition for understanding the self diffusion of polymer chains, additional constraints on the chain backbones are necessary for realistic penetrant diffusion to be modeled. We have also shown that the very signature of penetrant motion, as quantified by the functions D(d) and Z(t), changes as the chains are varied from the liquid-like freely jointed chains to the polymer-like freely rotating chains.

Although central to our analysis, neither D nor Z(t) were straightforward to calculate. The diffusion coefficient can be found either through $<R^2(t)>$ and equation (2.7), or through Z(t) and the Green-Kubo relation given in equation (2.9). We have employed both methods and find good agreement. In previous studies on simple liquids, the Green-Kubo method of determining the diffusion coefficient has often been criticized as being a less accurate and a more computational intensive path to the diffusion constant. There is some truth in this for simple liquids, where the long time tail of the velocity autocorrelation function is still fairly large when increasingly poor statistics mask the form of the function's tail. Indeed, we find that this is true for the highly flexible chains; however, for the freely rotating chains, Z(t) decays more rapidly and provides a convenient path for the calculation of D.

For highly detailed polymer models, we expect Z(t) to be particularly appealing. For these systems, the non-Fickian regime persists to long time making the calculation of D through $<R^2(t)>$ impractical. Parallel processing methods are not of great advantage here since runs must be performed for long times into the Fickian regime, and multiple short trajectories cannot be substituted. On the other hand, the timescale of Z(t) is that of a single hop, and the difficulty is the compilation of sufficient statistics. Consequently, averaging over many short, independent runs can, indeed, substitute for a single long run making this an ideal problem for parallelization.

The velocity autocorrelation function itself is worthy of more attention. The behavior of the velocity autocorrelation in simple liquids has had extensive theoretical treatment, but the function's behavior in non-collision driven systems has received much less attention. The current work presents strong evidence of the existence of a -5/2 tail for the diffusion of penetrants through polymer melts. In retrospect, this feature of the diffusion is not surprising. The local energy surface created by the polymer melt traps the penetrant for long, highly variable, periods of time. Consequently, the motion of the penetrant is much like the diffusion of a small particle through a lattice with a broad distribution of trapping times; a system which also yields a Z(t) with a -5/2 tail [7zz].

Appendix: Z(t) for a Particle in a Sphere

The stepped, velocity autocorrelation function for a single absolute velocity as plotted in figure 1A can be described by a sum of cosine terms:

$$Z^*(t,v) = \frac{8}{\pi^2} \sum_{n=1,3,5,\cdots}^{\infty} \frac{1}{n^2} \cos(nt^* v^*) \qquad (A.1)$$

where the reduced speed, v*, is the particle's speed, v, divided by its "most probable" speed, $c^*=(2kT/m)^{1/2}$. The reduced time, t*, is the time, t, divided by the period, $\tau=2\ell/c^*$; and ℓ is the sphere's diameter. In terms of the inherent MD time-step, t_0, τ is $\left(\sqrt{2}\,\ell/\sigma\right)t_0$.

To account for the distribution of particle speeds, the velocity autocorrelation function needs to be averaged over the Maxwell-Boltzmann distribution:

$$g(v^*) = \frac{4}{\sqrt{\pi}} v^{*2} \exp\left[-v^{*2}\right]. \qquad (A.2)$$

Averaging the velocity autocorrelation function over all possible speeds gives

$$Z^*(t) = \frac{32}{\pi^{5/2}} \sum_{n=1,3,5,\cdots}^{\infty} \frac{1}{n^2} \int_0^{\infty} \cos(nt^* v^*) v^{*2} \exp\left[-v^{*2}\right] dv^*. \qquad (A.3)$$

This can then be integrated to give,

$$Z^*(t) = \frac{8}{\pi^2} \sum_{n=1,3,5,\cdots}^{\infty} \frac{1}{n^2} \left[1 - \frac{(nt^*)^2}{2}\right] \exp\left[-\frac{(nt^*)^2}{4}\right] \qquad (A.4)$$

which converges rapidly with n. Retaining (and normalizing) the first term approximates $Z^*(t)$ reasonably well as

$$Z^*(t) = \left[1 - \frac{(t^*)^2}{2}\right] \exp\left[-\frac{(t^*)^2}{4}\right]. \qquad (A.5)$$

As discussed in the body of the paper, the Laplace transform of $Z^*(t)$,

$$\tilde{Z}(p) = \int_0^\infty Z^*(p) \exp(-pt)\, dt \qquad (A.6)$$

is also of interest. The transform of (A.4) yields

$$\tilde{Z}(p) = \frac{8\tau}{\pi^2} \sum_{n=1,3,5,\cdots}^{\infty} \frac{2p^*}{n^4}\left[1 - \frac{\sqrt{\pi}}{n} p^* \exp\left(\frac{p^{*2}}{n^2}\right) \operatorname{erfc}\left(\frac{p^*}{n}\right)\right] \qquad (A.7)$$

where p is the Laplace index; p^* is p times τ; and erfc(x) is the complimentary error function (i.e., 1 minus the error function). This is well approximated by the transform of (A.5) which yields:

$$\tilde{Z}(p) = 2\tau p^*\left[1 - \sqrt{\pi} p^* \exp\left(p^{*2}\right) \operatorname{erfc}(p^*)\right]. \qquad (A.8)$$

Integration of equation (A.6) by parts gives the asymptotic behavior of $\tilde{Z}(p) = 1/p + O(1/p^2)$. On the other hand, for small p, the exponential in equation (A.6) can be expanded as 1-pt+... . This leads to the small p expression of

$$\tilde{Z}(p) = 2\tau p^*\left[1 - \sqrt{\pi} p^*\right] + O\left(p^3\right). \qquad (A.9)$$

As a rational approximation of equation (A.8), we use

$$\tilde{Z}(p) = \tau \frac{p^*}{(A+p^*)^2}\left[1+B\frac{p^*}{(A+p^*)^2}\right] \qquad (A.10)$$

where A=0.8 and B=1.8. This captures the correct asymptotic behavior as well as the correct peak location and height (p_{max}=0.8/τ and $\tilde{Z}_{max}$=0.488τ), although only approximating the small p behavior. By forcing the large p behavior to be similar, the period of the trapped particle's vibration can be extracted from $\tilde{Z}(p)$ when there is a well defined maximum as there is for of K=500. In this case τ is 0.0851 t_0 or about 20 MD moves. Moreover, this implies that a K=500 penetrant moves only a short distance, ℓ=0.06 σ, before reversing its direction. In other words, the cavity constraining the penetrant is less than a tenth of a σ larger than the particle or about 1.06 σ in width.

The memory function can be found through equation (3.4). The approximate expression for $\tilde{Z}(p)$ given in equation (A.9) implies that ζ approaches 2A/τ for large p and $A^2/\tau p^*$ for small p. In figure 11vv, the long time behavior of the $\tilde{Z}(p)$ from simulation for K=500 is fitted to the numerical results of equation (A.7) in the long time tail. In figure 12vv, it can be seen that the K=500 memory function also converges to the ζ of the fully trapped particle at relatively short p.

Acknowledgement:

One of us (J.D.M.) is indebted to Randall LaViolette for useful discussions concerning diffusion in atomic systems.

References

1zz) F. Muller-Plathe, J. Chem. Phys. **96**, 3200 (1992).

2zz) A. A. Gusev and U. W. Suter, J. Chem. Phys. **99**, 2228 (1993).

3zz) P. V. K. Pant and R. H. Boyd, Macromolecules **25**, 494 (1992); P. V. K. Pant and R. H. Boyd, Macromolecules **26**, 679 (1993).

4zz) S. Sunderrajan, C.K. Hall, B.D. Freeman, J. Chem. Phys., **105**, 1621 (1996); **107**, 10714 (1997); A. P. Thompson, D.M. Ford, G.S. Heffelfinger, JCP **109**, 6406 (1998); D.M. Ford, G.S. Heffelfinger, Mol. Phys. **94**, 673 (1998); G.S. Heffelfinger, Mol. Phys. **94**, 659 (1998).

5zz) P.A. Netz and T. Dorfmuler, J. Chem. Phys. **103** 9074 (1995).

6zz) H. Takeuchi and K. Okasaki, J. Chem. Phys. **92**, 5643 (1990); H. Takeuchi, J. Chem. Phys. **93**, 2062 (1990); H. Takeuchi, J. Chem. Phys. **93**, 4490 (1990); H. Takeuchi, R.-J. Roe, and J.E. Mark, J. Chem Phys. **93**, 9042 (1990); M. L. Greenfield and D. N. Theodorou, Macromolecules **26**, 5461 (1993).

7zz) K. Kundu and P. Phillips, Phys. Rev. A **35**, 857 (1987); J. W. Haus and K. W. Kehr; Phys. Rev. A **37**, 4522, (1988); K. Kundu and P. Phillips, Phys. Rev. A **37**, 4524 (1988).

8zz) B.J. Alder and T.E. Wainwright, Phys. Rev. A **1**, 18 (1970); D. Levesque, L. Verlet, and J. Kurkijarvi, Phys. Rev. A **7**, 1690 (1973); G. F. Mazenko, Phys. Rev. A **7**, 222 (1973); J.R. Mehaffey and R.I. Cukier, Phys. Rev. A **17**, 1181 (1978).

9zz) C.R. Wilke and P. Chang, A.I.Ch.E. Journal **1**, 264 (1955); Reid, Prausnitz and Sherwood, op. Cit.

10zz) J.-P. Hansen and I. R. McDonald, *Theory of Simple Liquids* (Academic Press, second edition, 1991); J.-P. Boon and S. Yip, *Molecular Hydrodynamics* (Dover, 1991); H. Risken, *The Fokker-Plank Equation* (Springer-Verlag, 1989)

11zz) J. Brandup and E. H. Immergut, ed. *Polymer Handbook.* (John Wiley and Sons, New York, third edition, 1989).

12zz) P. Meares, J. Am. Chem. Soc., **76**, 3415 (1954); Brandt and Anysas, J. Appl. Polym. Sci., **7**, 1919 (1963).

13zz) G. S. Grest and K. Kremer, Phys. Rev. A **33**, 3628 (1986); K. Kremer and G. S. Grest, Phys. Rev. Lett. **61**, 566 (1988); J. Chem. Phys. **92**, 5057 (1990).

14zz) C. S. Stevenson, J. D. McCoy, J. G. Curro, and S. J. Plimpton, J. Chem. Phys., 103, 1200 (1995); C. S. Stevenson, J. D. McCoy, J. G. Curro, and S. J. Plimpton, J. Chem. Phys. **103**, 1208 (1995). P.A. Tillman, D.R. Rottach, J.D. McCoy, S.J. Plimpton, and J.G. Curro, J. Chem. Phys., **107** 4024 (1997), **109** 806 (1998).

15zz) J. A. Barker and D. Hendersen, Rev. Mod. Phys. **48**, 587 (1976).

16zz) J.L. Budzien, J.D. McCoy, J.G. Curro, R.A. LaViollette, and E.S. Peterson, Macromolecules **31**, 6669 (1998); **31**, 8653 (1998).

17zz) M.P. Allen and D.J. Tildesley, *Computer Simulation of Liquids* (Academic Press, 1986).

18zz) M. A. Wilson, A. Pohorille, and L.R. Pratt, J. Chem. Phys. **83** 5832 (1985).

19zz) N. Corngold, Phys. Rev. A, **6** 1570 (1972).

TableI: Diffusion coefficients in units of σ^2/t_0 obtained from $<R^2>$ analysis.

	K=0	0.5	1.0	10	20	100	300	500
d= 0.8	0.150	0.13	0.092	0.050	0.035	0.018	0.029	0.018
0.9	0.137	0.10		0.030	0.026	0.017	0.013	0.015
1.0	0.100	0.085	0.075	0.025	0.021	0.011	0.011	0.011
1.1	0.095	0.080	0.057	0.017	0.015	0.013	0.0067	0.0067
1.2	0.070	0.065	0.050	0.015	0.010	0.0065	0.0046	0.0041

TableI: Diffusion coefficients in units of σ^2/t_0 obtained from $\langle R^2 \rangle$ analysis.

	K=0	0.5	1.0	10	20	100	300	500
d= 0.8	0.150	0.13	0.092	0.050	0.035	0.018	0.020	0.018
0.9	0.137	0.10	0.085	0.030	0.026	0.017	0.013	0.015
1.0	0.100	0.085	0.075	0.025	0.021	0.011	0.011	0.011
1.1	0.095	0.080	0.057	0.017	0.015	0.013	0.0067	0.0067
1.2	0.070	0.065	0.050	0.015	0.010	0.0065	0.0046	0.0041

TableII: Power law exponents for the long time tail of Z(t).

	K=0	0.5	1.0	10	20	100	300	500
d= 0.8	-1.5	-1.5	-1.9	-2.2	-2.2	-2.1	-2.5	-2.5
0.9	-1.5	-1.7	-1.5	-1.9	-2.3	-2.1	-2.5	-2.5
1.0	-1.5	-1.5	1.5	-2.0	-2.1	-2.3	-2.5	-2.5
1.1	-1.5	-1.3	-1.1	-1.9	-2.0	-2.1	-2.5	-2.5
1.2	-1.5	-1.3	-1.2	-1.8	-1.9	-2.1	-2.5	-2.3

Table III: Diffusion coefficients in units of σ^2/t_0 obtained from Z(t) analysis.

	K=0	0.5	1.0	10	20	100	300	500
d= 0.8	0.14	0.11	0.107	0.043	0.034	0.021	0.019	0.017
0.9	0.11	0.099	0.079	0.032	0.027	0.016	0.013	0.016
1.0	0.093	0.096	0.063	0.024	0.019	0.014	0.013	0.012
1.1	0.088	0.069	0.057	0.019	0.014	0.014	0.010	0.0089
1.2	0.067	0.057	0.046	0.014	0.0088	0.0071	0.0064	0.0065

Figure captions

1) The velocity autocorrelation function for a particle in a 1-dimensional box. A) $v(t) \bullet v(0)$ where t=0 is just after a collision with a wall. B) The average of $v(t) \bullet v(t_0)$ over all starting times. C) The velocity autocorrelation function of a trapped particle (solid line) which is obtained by averaging (B) over the Maxwell-Boltzmann velocity distribution and (dashed line) of a Brownian particle.

2) The logarithm of the squared displacement of d=1 penetrants vs. the logarithm of the reduced time. The upper curve is the K=0 melt and the lower, the K=500 melt.

3) The velocity autocorrelation functions of penetrant and polymer site. The d=1 penetrant $Z^*(t)$ is dashed and the K=0 polymer $Z^*(t)$ is solid.

4) Integration of the velocity autocorrelation function of d=1 penetrants in both K=0 (solid line) and K=500 (dashed line) polymer melts.

5) The variation of the diffusion constant with penetrant diameter. Circles refer to the K=0 simulation. Triangles represent diffusion constants of various acids in toluene, from Wilke-Chang [9zz]. In both cases, the fitted slope is –1.8.

6) The variation of the diffusion constant with penetrant diameter. The filled circles represent the K=500 case; the open circles, the K=0 case; and the X's and +'s represent experimental results for the diffusion of light gases through high density and low density polyethylene, respectively [11zz].

7) Velocity autocorrelation function for d=1 penetrants in a K=0 polymer. The main figure shows the tail of $Z^*(t)$ which is fit by a $t^{-3/2}$ power law. The full $Z^*(t)$ is shown in the insert.

8) Velocity autocorrelation function for d=1 penetrants in a K=500 polymer. The main figure shows the tail of Z(t) which is fit by a $t^{-5/2}$ power law. The full Z(t) is shown in the insert.

9) Cross-plot of the diffusion coefficients calculated by $\langle R^2 \rangle$ and Z(t) routes. The line represents perfect agreement.

10) Force autocorrelation functions. The solid line is for d=1 penetrants in a K=0 polymer; the dashed, in a K=500 polymer.

11) Velocity autocorrelation functions of d=1 penetrants in Laplace space. The upper solid line is for the K=0 polymer; and the lower solid line, for the K=500 polymer. The upper dotted line is for Brownian motion with a large p limit set to the K=0 result. The lower dotted line is for the fully trapped particle with its large p limit set to the K=500 result.

12) Memory functions of d=1 penetrants in Laplace space. The upper solid line is for the K=500 polymer; and the lower solid line, for the K=0 polymer. The dotted line is for the fully trapped particle.

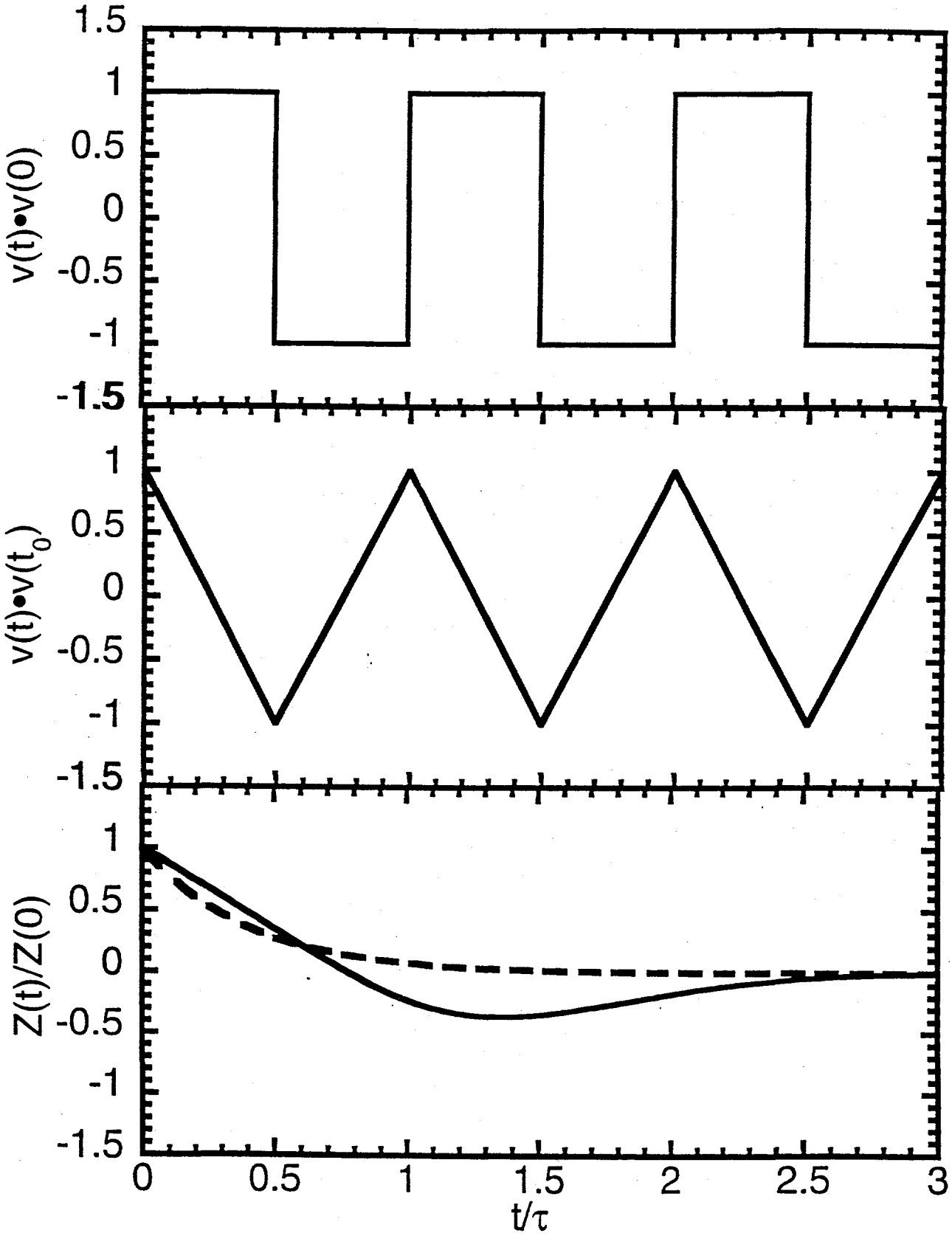
1.5
1
0.5
0
-0.5
-1
-1.5
v(t)•v(0)
v(t)•v(t0)
Z(t)/Z(0)
0
0.5
1
1.5
2
2.5
3
t/τ

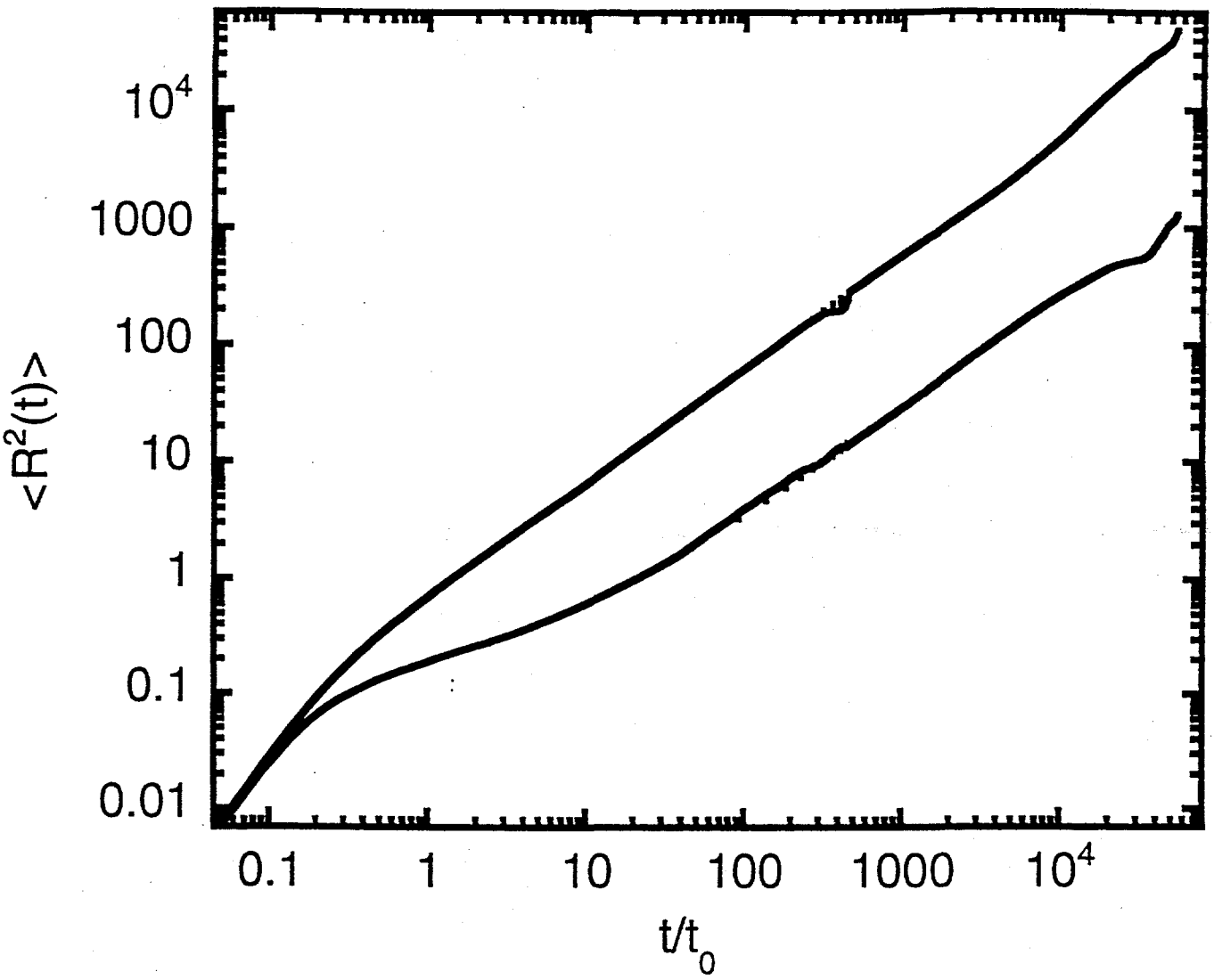
10^4
1000
100
10
1
0.1
0.01
$\langle R^2(t) \rangle$
0.1
1
10
100
1000
10^4
t/t_0

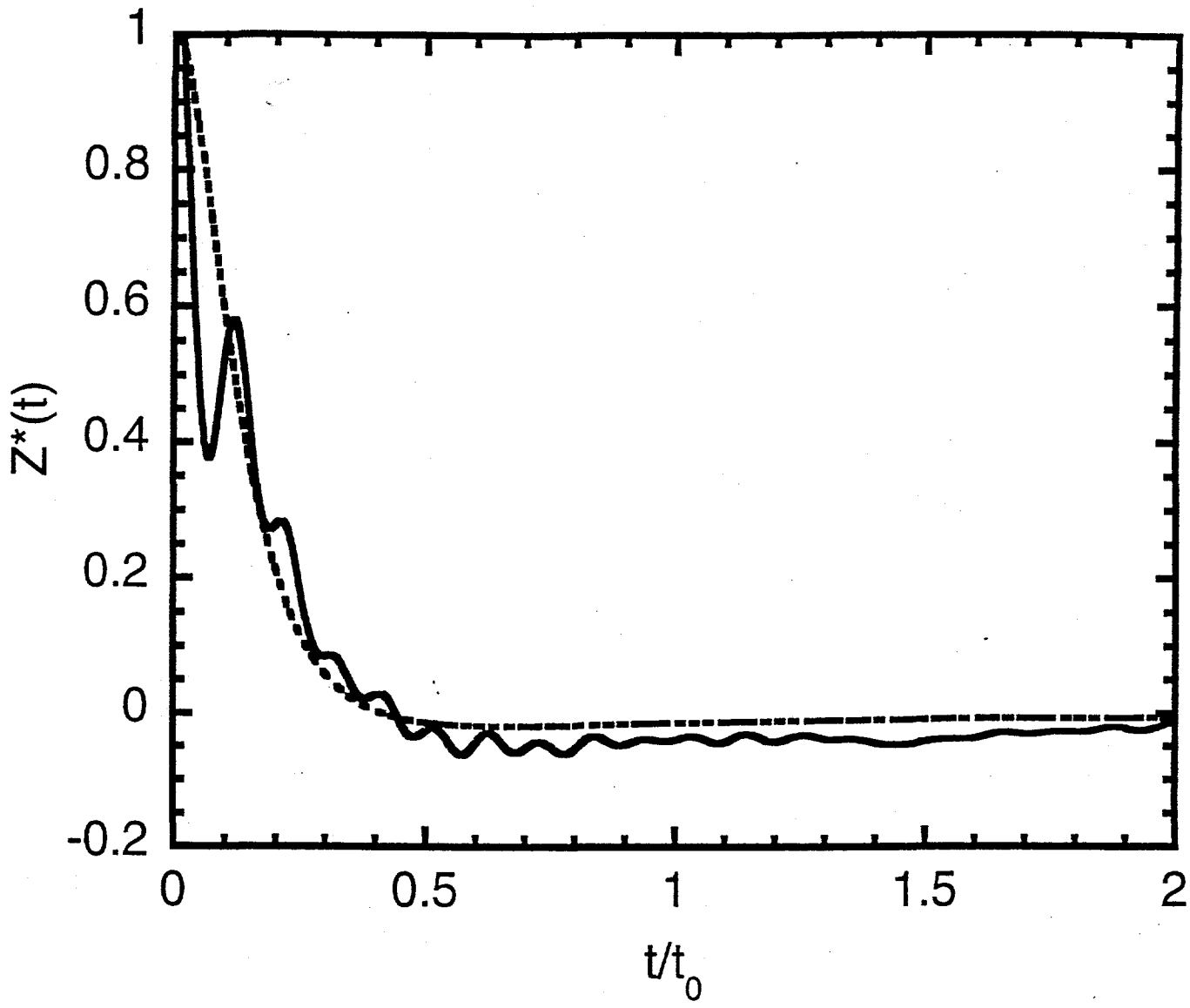
1
0.8
0.6
0.4
0.2
0
-0.2
Z*(t)
0
0.5
1
1.5
2
t/t0

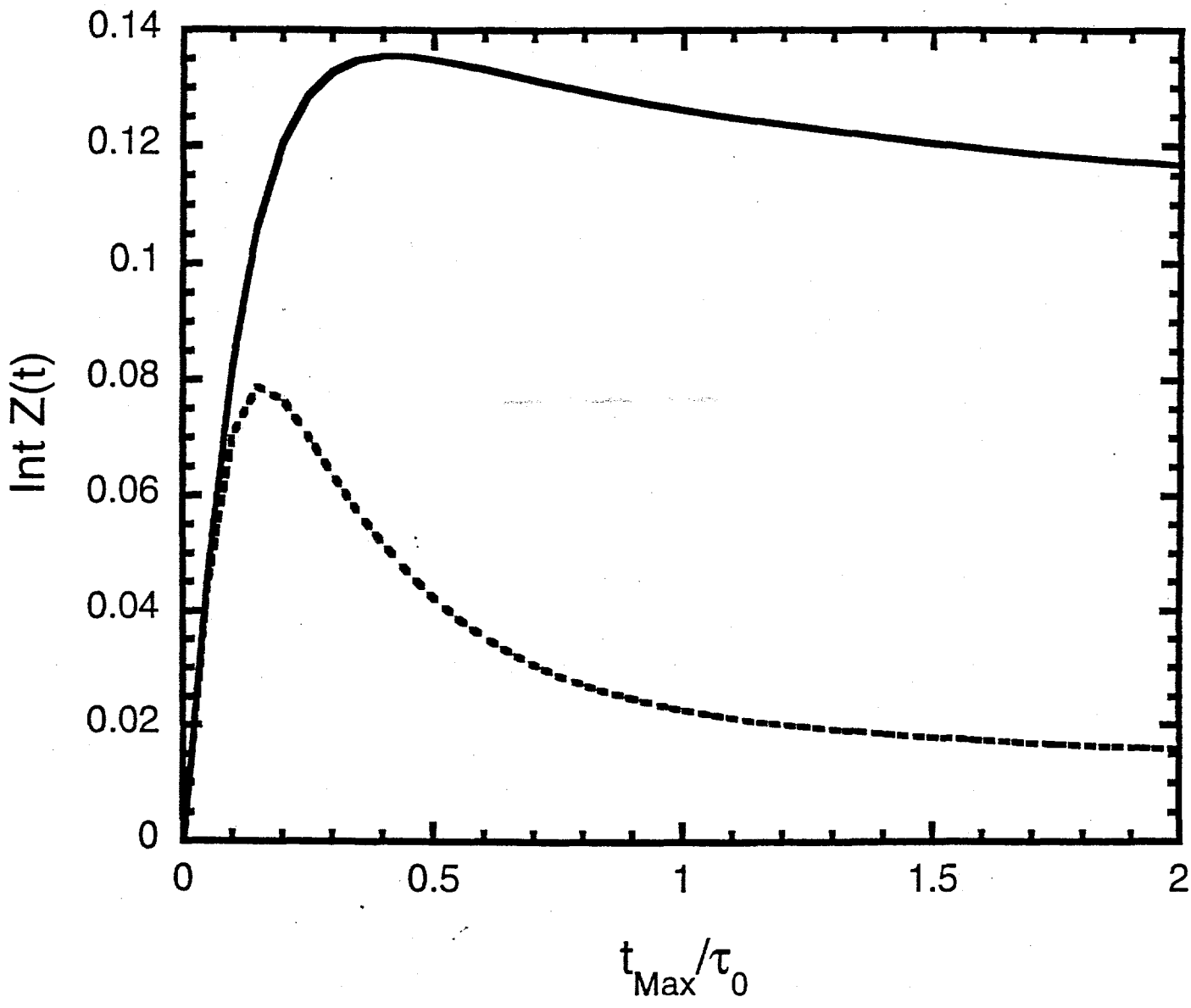
0.14
0.12
0.1
0.08
0.06
0.04
0.02
0
Int Z(t)
0
0.5
1
1.5
2
t_{Max}/τ_0

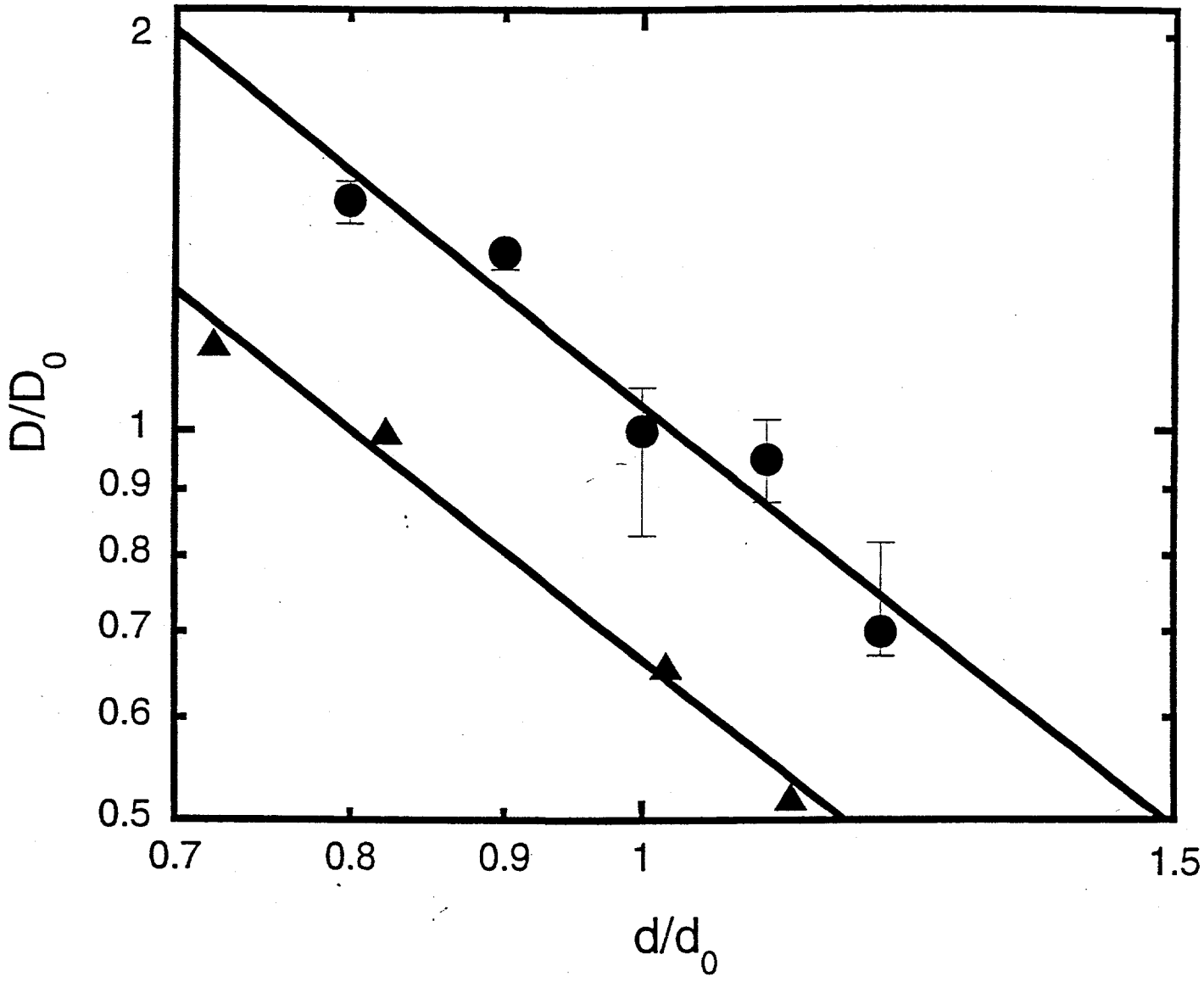
2
1
0.9
0.8
0.7
0.6
0.5
D/D0
0.7
0.8
0.9
1
1.5
d/d0

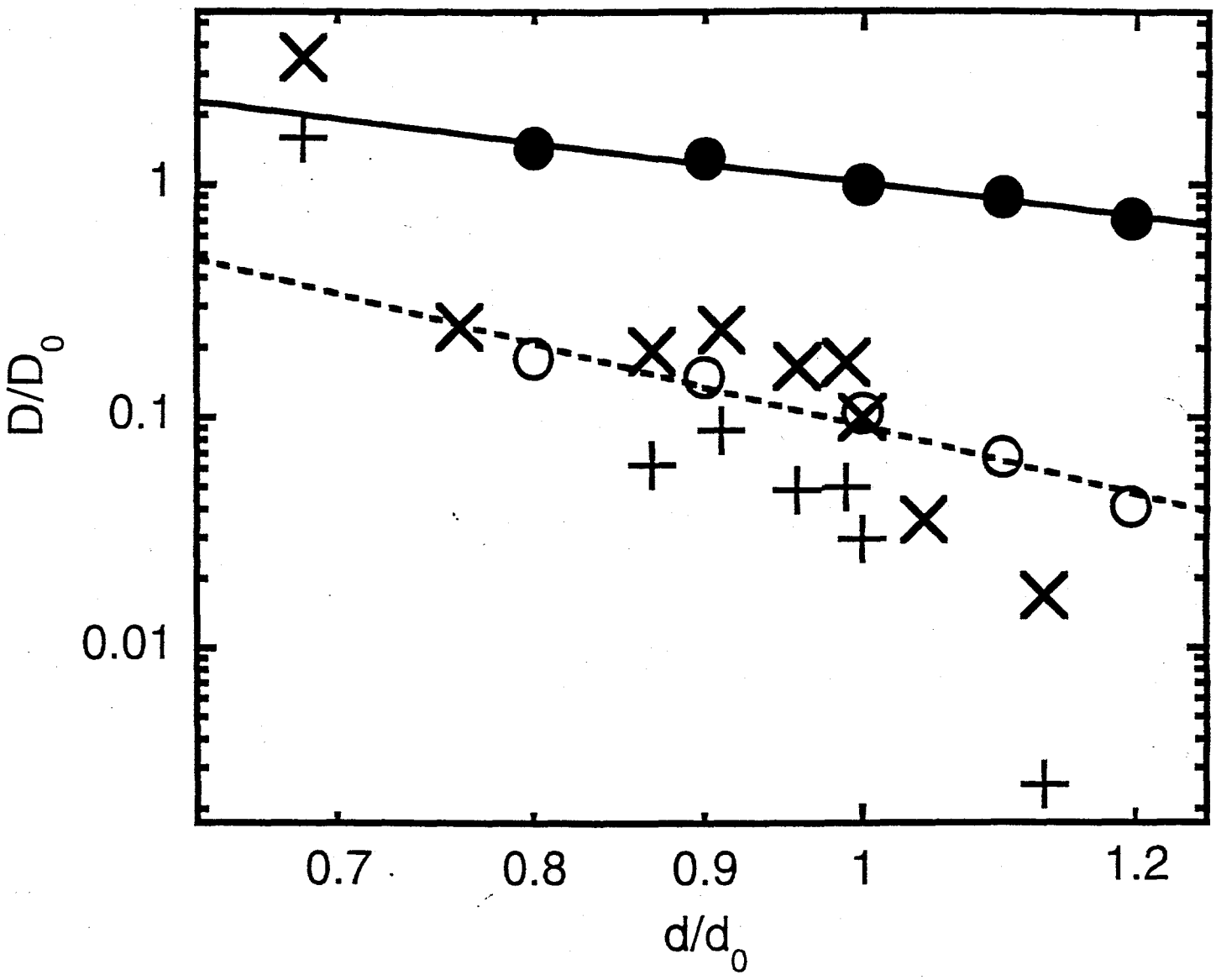
D/D0
1
0.1
0.01
0.7
0.8
0.9
1
1.2
d/d0

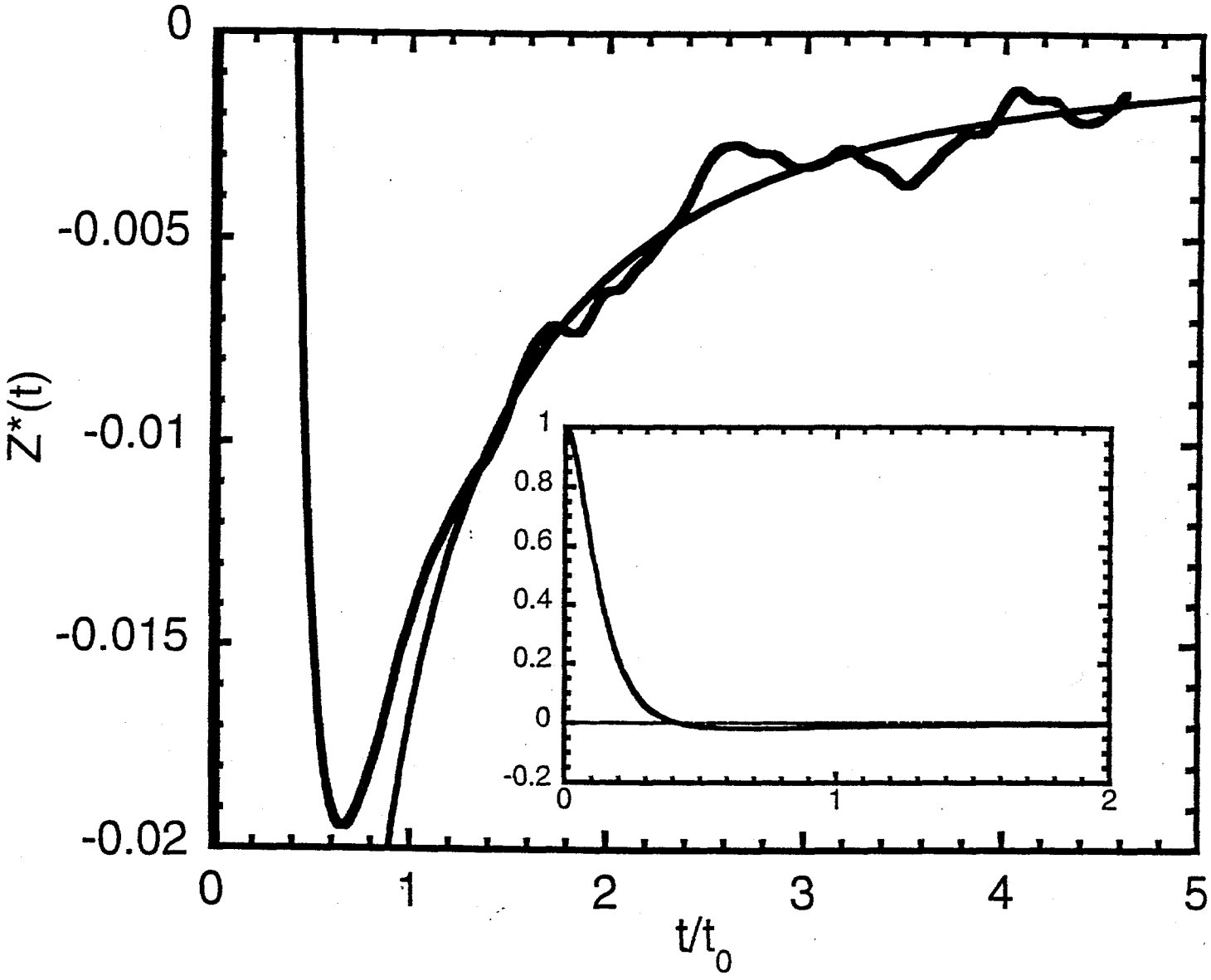
0
-0.005
-0.01
-0.015
-0.02
Z*(t)
0
1
2
3
4
5
t/t0
1
0.8
0.6
0.4
0.2
0
-0.2
0
1
2

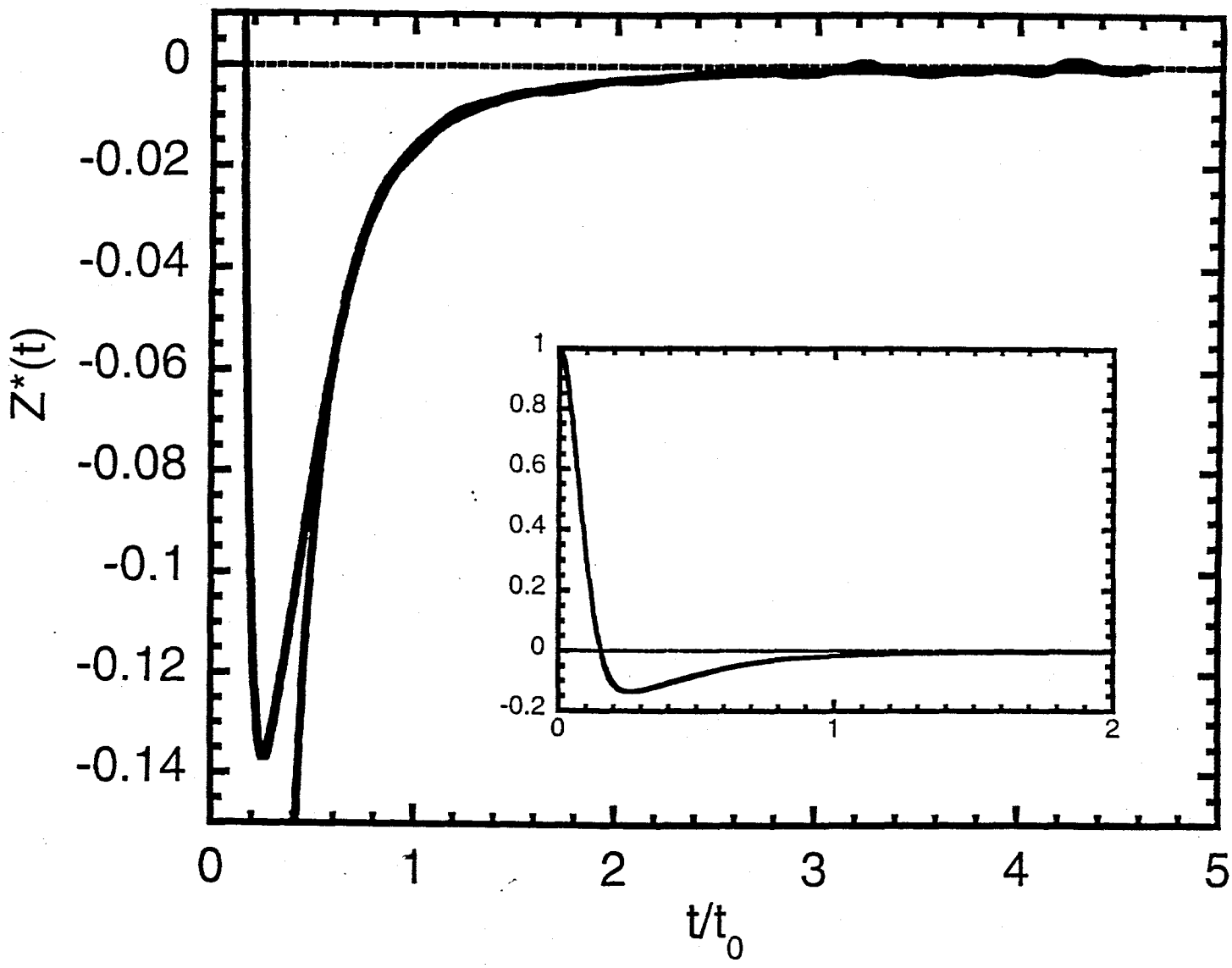
0
-0.02
-0.04
-0.06
-0.08
-0.1
-0.12
-0.14
Z*(t)
0
1
2
3
4
5
t/t0
1
0.8
0.6
0.4
0.2
0
-0.2
0
1
2

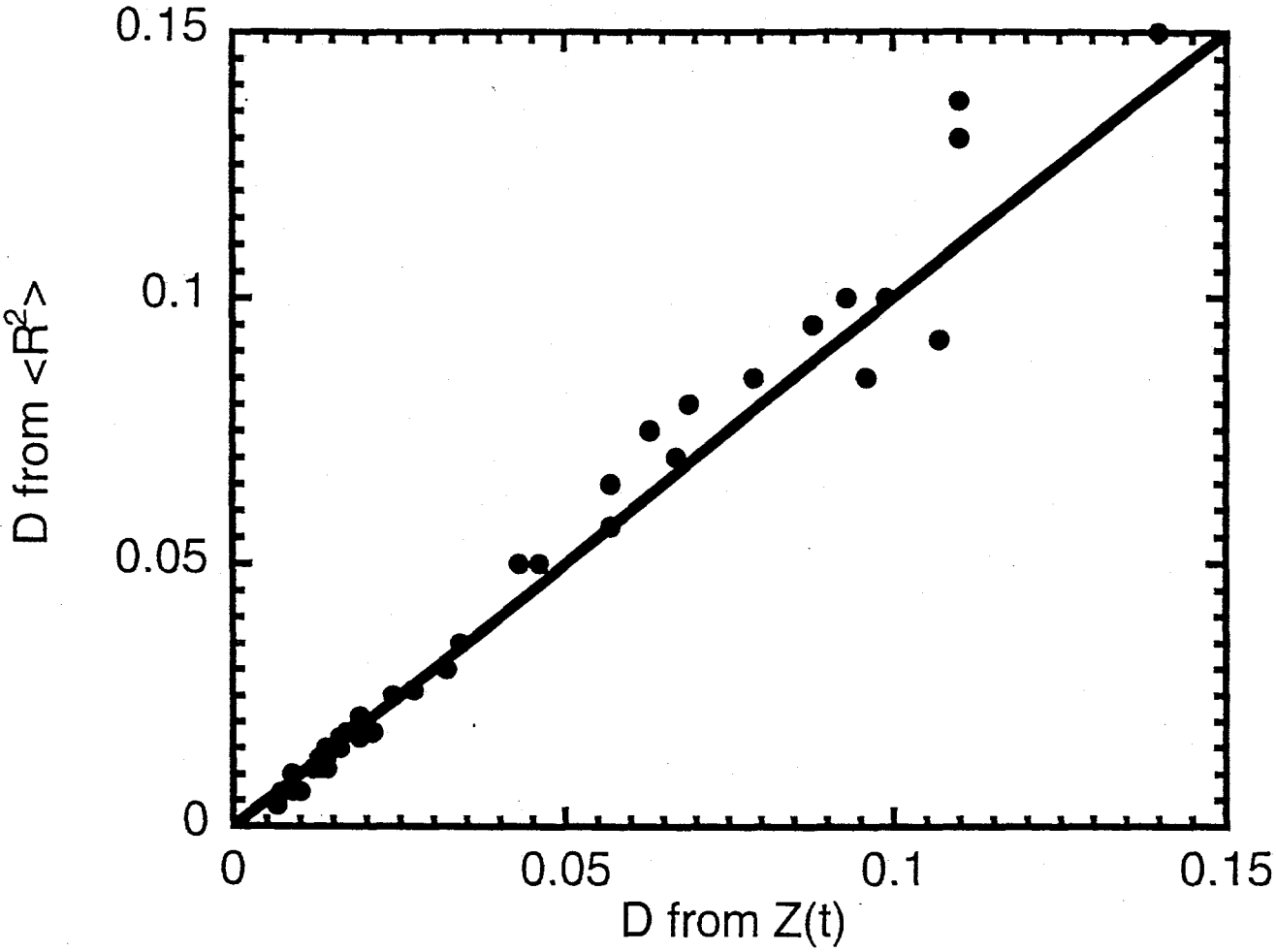
0.15
0.1
0.05
0
D from <R²>
0
0.05
0.1
0.15
D from Z(t)

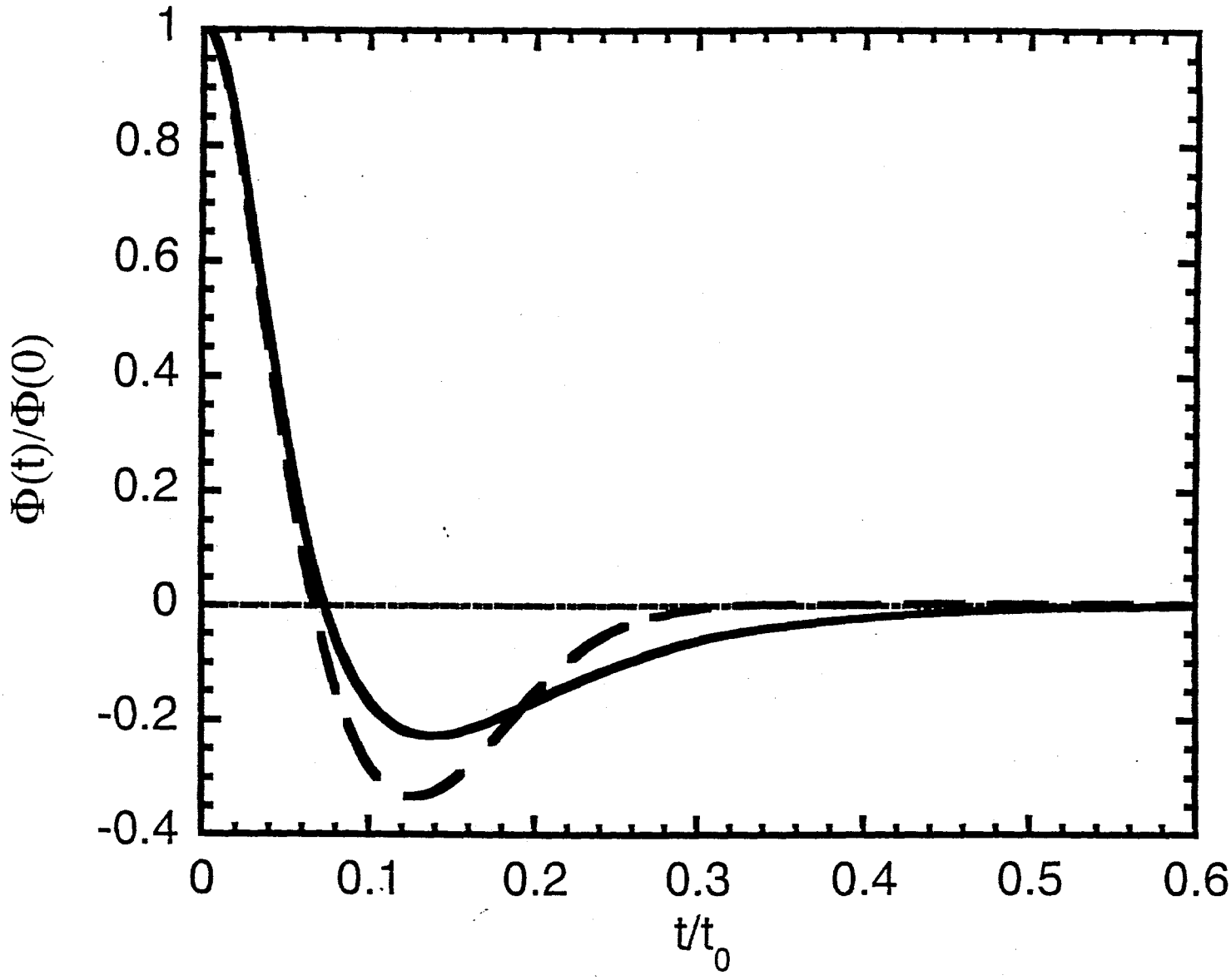
1
0.8
0.6
0.4
0.2
0
-0.2
-0.4
Φ(t)/Φ(0)
0
0.1
0.2
0.3
0.4
0.5
0.6
t/t0

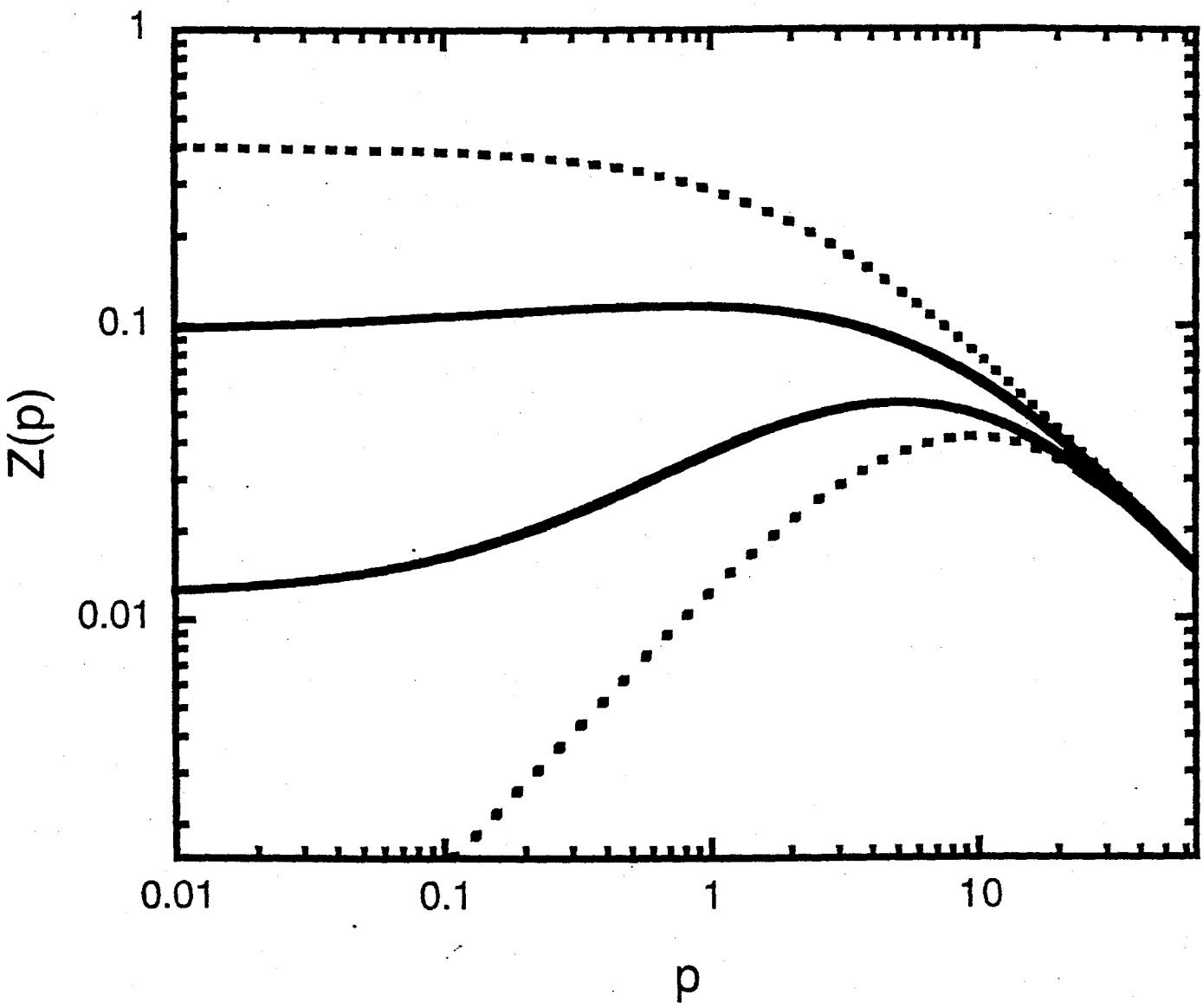
1
0.1
0.01
Z(p)
0.01
0.1
1
10
p

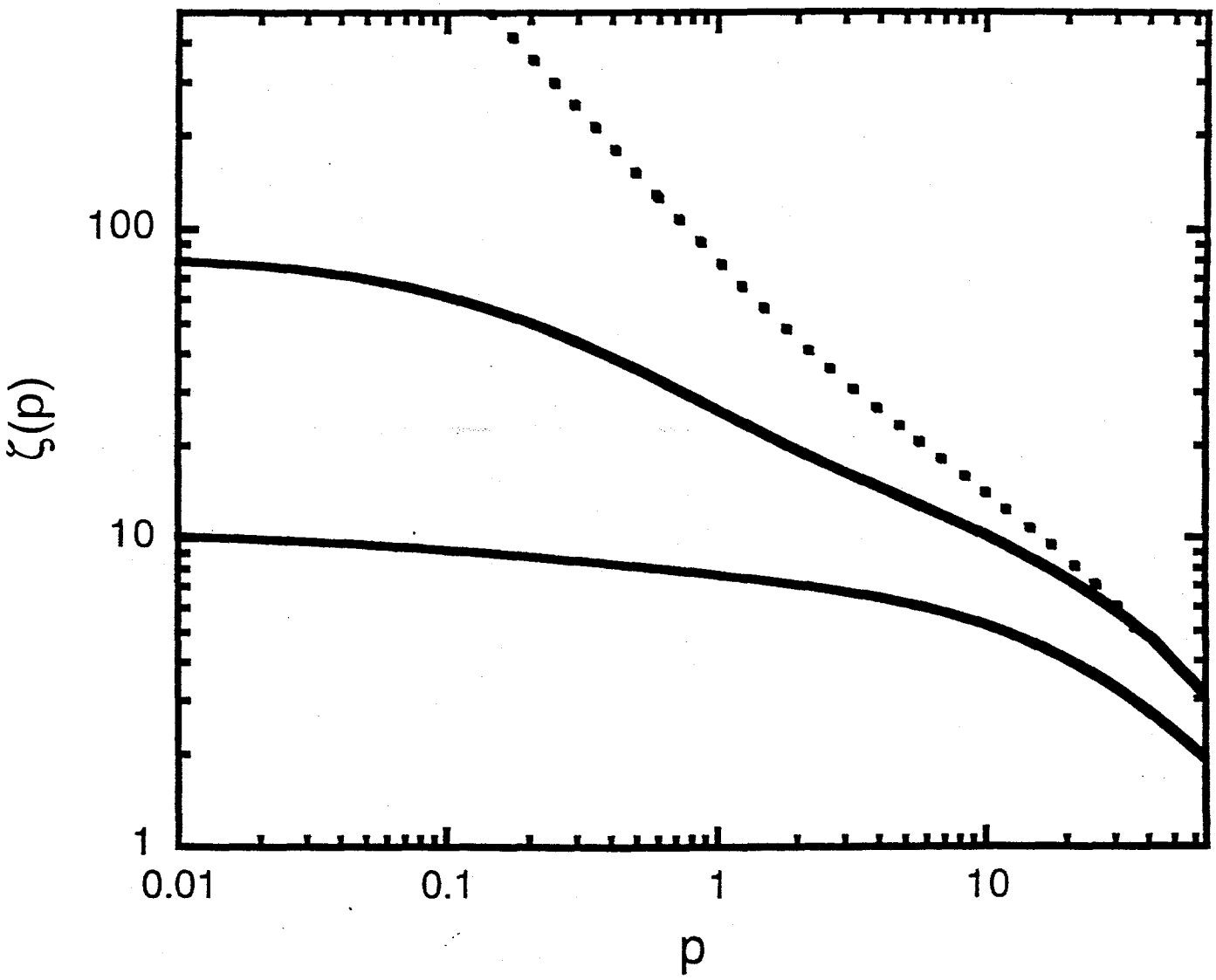
100
10
1
ζ(p)
0.01
0.1
1
10
p